the N-terminal Dbl homology domain of the nucleotide exchange factor Trio. Cell **95**:269–277.

24. **Maeda, N., M. Niinobe, and K. Mikoshiba.** 1990. A cerebellar Purkinje cell marker P400 protein is an inositol 1,4,5-trisphosphate (InsP3) receptor protein. Purification and characterization of InsP3 receptor complex. EMBO J. **9**:61–67.

25. **McPherson, C. E., B. A. Eipper, and R. E. Mains.** 2005. Multiple novel isoforms of Trio are expressed in the developing rat brain. Gene **347**:125–135.

26. **Michaelson, D., J. Silletti, G. Murphy, P. D'Eustachio, M. Rush, and M. R. Philips.** 2001. Differential localization of Rho GTPases in live cells: regulation by hypervariable regions and RhoGDI binding. J. Cell Biol. **152**:111–126.

27. **Miura, K., S. Miyazawa, S. Furuta, J. Mitsushita, K. Kamijo, H. Ishida, T. Miki, K. Suzukawa, J. Resau, T. D. Copeland, and T. Kamata.** 2001. The Sos1-Rac1 signaling. Possible involvement of a vacuolar H⁺-ATPase E subunit. J. Biol. Chem. **276**:46276–46283.

28. **Mohrmann, K., and P. van der Sluijs.** 1999. Regulation of membrane transport through the endocytic pathway by rabGTPases. Mol. Membr. Biol. **16**:81–87.

29. **Mukherjee, S., R. N. Ghosh, and F. R. Maxfield.** 1997. Endocytosis. Physiol. Rev. **77**:759–803.

30. **Mullen, R. J., E. M. Eicher, and R. L. Sidman.** 1976. Purkinje cell degeneration, a new neurological mutation in the mouse. Proc. Natl. Acad. Sci. USA **73**:208–212.

31. **Munro, S., and H. R. Pelham.** 1986. An Hsp70-like protein in the ER: identity with the 78 kd glucose-regulated protein and immunoglobulin heavy chain binding protein. Cell **46**:291–300.

32. **Nielsen, E., F. Severin, J. M. Backer, A. A. Hyman, and M. Zerial.** 1999. Rab5 regulates motility of early endosomes on microtubules. Nat. Cell Biol. **1**:376–382.

33. **Nishimura, T., Y. Fukata, K. Kato, T. Yamaguchi, Y. Matsuura, H. Kamiguchi, and K. Kaibuchi.** 2003. CRMP-2 regulates polarized Numb-mediated endocytosis for axon growth. Nat. Cell Biol. **5**:819–826.

34. **Nordquist, D. T., C. A. Kozak, and H. T. Orr.** 1988. cDNA cloning and characterization of three genes uniquely expressed in cerebellum by Purkinje neurons. J. Neurosci. **8**:4780–4789.

35. **O'Brien, S. P., K. Seipel, Q. G. Medley, R. Bronson, R. Segal, and M. Streuli.** 2000. Skeletal muscle deformity and neuronal disorder in Trio exchange factor-deficient mouse embryos. Proc. Natl. Acad. Sci. USA **97**:12074–12078.

36. **Otomo, A., S. Hadano, T. Okada, H. Mizumura, R. Kunita, H. Nishijima, J. Showguchi-Miyata, Y. Yanagisawa, E. Kohiki, E. Suga, M. Yasuda, H. Osuga, T. Nishimoto, S. Narumiya, and J. E. Ikeda.** 2003. ALS2, a novel guanine nucleotide exchange factor for the small GTPase Rab5, is implicated in endosomal dynamics. Hum. Mol. Genet. **12**:1671–1687.

37. **Penzes, P., A. Beeser, J. Chernoff, M. R. Schiller, B. A. Eipper, R. E. Mains,**

and **R. L. Huganir.** 2003. Rapid induction of dendritic spine morphogenesis by trans-synaptic ephrinB-EphB receptor activation of the Rho-GEF kalirin. Neuron **37**:263–274.

38. **Penzes, P., R. C. Johnson, R. Sattler, X. Zhang, R. L. Huganir, V. Kambampati, R. E. Mains, and B. A. Eipper.** 2001. The neuronal Rho-GEF Kalirin-7 interacts with PDZ domain-containing proteins and regulates dendritic morphogenesis. Neuron **29**:229–242.

39. **Pfeffer, S.** 2003. Membrane domains in the secretory and endocytic pathways. Cell **112**:507–517.

40. **Ren, M., G. Xu, J. Zeng, C. De Lemos-Chiarandini, M. Adesnik, and D. D. Sabatini.** 1998. Hydrolysis of GTP on rab11 is required for the direct delivery of transferrin from the pericentriolar recycling compartment to the cell surface but not from sorting endosomes. Proc. Natl. Acad. Sci. USA **95**:6187–6192.

41. **Rico, B., H. E. Beggs, D. Schahin-Reed, N. Kimes, A. Schmidt, and L. F. Reichardt.** 2004. Control of axonal branching and synapse formation by focal adhesion kinase. Nat. Neurosci. **7**:1059–1069.

42. **Schmidt, A., and A. Hall.** 2002. Guanine nucleotide exchange factors for Rho GTPases: turning on the switch. Genes Dev. **16**:1587–1609.

43. **Sha, B., S. E. Phillips, V. A. Bankaitis, and M. Luo.** 1998. Crystal structure of the Saccharomyces cerevisiae phosphatidylinositol-transfer protein. Nature **391**:506–510.

44. **Shima, Y., M. Kengaku, T. Hirano, M. Takeichi, and T. Uemura.** 2004. Regulation of dendritic maintenance and growth by a mammalian 7-pass transmembrane cadherin. Dev. Cell **7**:205–216.

45. **Simonsen, A., R. Lippe, S. Christoforidis, J. M. Gaullier, A. Brech, J. Callaghan, B. H. Toh, C. Murphy, M. Zerial, and H. Stenmark.** 1998. EEA1 links PI(3)K function to Rab5 regulation of endosome fusion. Nature **394**:494–498.

46. **Somsel Rodman, J., and A. Wandinger-Ness.** 2000. Rab GTPases coordinate endocytosis. J. Cell Sci. **113**(Pt. 2):183–192.

47. **Symons, M., and N. Rusk.** 2003. Control of vesicular trafficking by rho GTPases. Curr. Biol. **13**:R409–R418.

48. **Tanaka, M., N. Maeda, M. Noda, and T. Marunouchi.** 2003. A chondroitin sulfate proteoglycan PTPζ/RPTPβ regulates the morphogenesis of Purkinje cell dendrites in the developing cerebellum. J. Neurosci. **23**:2804–2814.

49. **Tanaka, M., A. Tomita, S. Yoshida, M. Yano, and H. Shimizu.** 1994. Observation of the highly organized development of granule cells in rat cerebellar organotypic cultures. Brain Res. **641**:319–327.

50. **van der Luit, A. H., M. Budde, P. Ruurs, M. Verheij, and W. J. van Blitterswijk.** 2002. Alkyl-lysophospholipid accumulates in lipid rafts and induces apoptosis via raft-dependent endocytosis and inhibition of phosphatidylcholine synthesis. J. Biol. Chem. **277**:39541–39547.

51. **Wang, Y. L., W. Liu, E. Wada, M. Murata, K. Wada, and I. Kanazawa.** 2005. Clinico-pathological rescue of a model mouse of Huntington's disease by siRNA. Neurosci. Res. **53**:241–249.

Parkin Potentiates ATP-Induced Currents Due to Activation of P2X Receptors in PC12 Cells

AYUMI SATO,[1] YUKIKO ARIMURA,[1] YOSHIMASA MANAGO,[1] KAORI NISHIKAWA,[2] KUMIKO AOKI,[2]
ETSUKO WADA,[2] YASUYUKI SUZUKI,[2] HITOSHI OSAKA,[2,3] RIEKO SETSUIE,[1,2] MIKAKO SAKURAI,[1,2]
TAIJU AMANO,[1,2] SHUNSUKE AOKI,[2,4] KEIJI WADA,[2] AND MAMI NODA[1]*

[1]Laboratory of Pathophysiology, Graduate School of Pharmaceutical Sciences,
Kyushu University, Fukuoka, Japan
[2]Department of Degenerative Neurological Diseases, National Institute of Neuroscience,
National Center of Neurology and Psychiatry, Tokyo, Japan
[3]Information and Cellular Function, PRESTO, Japan Science and Technology Corporation (JST),
Kawaguchi, Saitama, Japan
[4]NEDO (New Energy and Industrial Technology Development Organization),
Kawasaki, Kanagawa, Japan

Loss-of-function mutations of the parkin gene causes an autosomal recessive juvenile-onset form of Parkinson's disease (AR-JP). Parkin was shown to function as a RING-type E3 ubiquitin protein ligase. However, the function of parkin in neuronal cells remains elusive. Here, we show that expression of parkin-potentiated adenosine triphosphate (ATP)-induced currents that result from activation of the P2X receptors which are widely distributed in the brain and involved in neurotransmission. ATP-induced inward currents were measured in mock-, wild-type or mutant (T415N)-parkin-transfected PC12 cells under the conventional whole-cell patch clamp configuration. The amplitude of ATP-induced currents was significantly greater in wild-type parkin-transfected cells. However, the immunocytochemical study showed no apparent increase in the number of P2X receptors or in ubiquitin levels. The increased currents were attenuated by inhibition of cAMP-dependent protein kinase (PKA) but not protein kinase C (PKC) or Ca^{2+} and calmodulin-dependent protein kinase (CaMKII). ATP-induced currents were also regulated by phosphatases and cyclin-dependent protein kinase 5 (CDK5) via dopamine and cyclic AMP-regulated phosphoprotein (DARPP-32), though the phosphorylation at Thr-34 and Thr-75 were unchanged or rather attenuated. We also tried to investigate the effect of α-synuclein, a substrate of parkin and also forming Lysine 63-linked multiubiquitin chains. Expression of α-synuclein did not affect the amplitude of ATP-induced currents. Our finding provides the evidence for a relationship between parkin and a neurotransmitter receptor, suggesting that parkin may play an important role in synaptic activity.   J. Cell. Physiol. 209: 172–182, 2006. © 2006 Wiley-Liss, Inc.

Recessive juvenile-onset form of Parkinson's disease (AR-JP) is the most frequent form of familial Parkinson's disease (PD). Mutations in the parkin gene were originally discovered from the linkage study of Japanese AR-JP families (Kitada et al., 1998). Thereafter its mutations have been found worldwide and parkin gene is now accepted as one of eight genes responsible for Parkinson's disease (see review by Cookson, 2005).

It has been demonstrated that parkin is associated with the ubiquitin–proteasome system. Wild-type parkin encodes for a protein-ubiquitin E3 ligase, which ubiquitinates many substrate proteins to enhance their degradation by the 26S proteasomes (Imai et al., 2000; Shimura et al., 2000; Zhang et al., 2000). As parkin mutations lose their E3 ligase activity, it is thought that accumulation of parkin substrate may lead to the selective death of catecholaminergic cell death (Ko et al., 2005) and familial-associated mutations differentially disrupt the solubility, localization, binding, and uniubiquitination properties of parkin (Sriram et al., 2005).

It is reported that parkin is localized on surface of synaptic vesicle membranes (Kubo et al., 2001). As substrates of parkin, some synaptic proteins were reported, such as synaptotagmin XI (Huynh et al., 2003), septin CDCrel-1 (Zhang et al., 2000), and synphylin1 (Lim et al., 2005), suggesting that parkin may have a neuronal function. However, the nature of this function is unknown. Therefore, we have investigated the effect of parkin on one of receptor channels that affect neurotransmitter secretion.

Adenosine triphosphate (ATP) and related nucleotides induce a release of catecholamines, including dopamine, in PC12 pheochromocytoma cells, a frequently used model for sympathetic neurons (Sela et al., 1991; Nakazawa and Inoue, 1992). ATP receptors are divided into two subtypes, P2X and P2Y receptors.

P2X receptors are ionotropic receptors and form cationic channels, while P2Y receptors are G-protein-coupled receptors. Recently, we have reported that P2X receptor-induced membrane currents were augmented by ubiquitin carboxy-terminal hydrolase L1 (UCH-L1), presumably due to upregulation of mono-ubiquitin level (Manago et al., 2005). Therefore, the ubiquitin–proteasome pathway is also implicated in the function of ATP receptors.

In the present study, we analyzed relationships between parkin and P2X receptors by expressing parkin or a familial-linked mutant parkin (T415N-parkin) which lacks ubiquitin E3 ligase activity in PC12 cells. This is the first evidence to show the relationship between physiological function of parkin and receptor channels involved in neurotransmitter secretion. These findings may help to understand the function of parkin in the nervous system and the mechanism of Parkinson's disease caused by dysfunction of parkin.

MATERIALS AND METHODS
Chemicals

RPMI-1640 medium, ATP-2Na, H-89 (N-[2-(p-bromoocinamylamino)ethyl]-5-isoquinolinesulfonamide), H-85, cheler-ythrine, roscovitine (2-(R)-(1-Ethyl-2-hydroxyethylamino)-6-benzylamino-9-isopropylpurine), and PD98059 (2'-Amino-3'-methoxyflavone) were from Sigma (St. Louis, MO). Nerve growth factor (NGF) and Lipofectamine 2000 were from Invitrogen (Carlsbad, CA). KN-93 (2-[N-(2-hydroxyethyl)]-N-(4-methoxybenzenesulfonyl))amino-N-(4-chlorocinnamyl)-N-methylbenzylamine) and okadaic acid was from Calbiochem (San Diego, CA).

Cell culture

PC12 Tet-off cells were grown in RPMI-1640 medium containing 5% fetal bovine serum (FBS) (Cell Culture Technologies, Lugano, Switzerland), 10% horse serum (HS) (Invitrogen), 100 units/ml penicillin (Life Technologies, Rockville, MD), and 100 µg/ml streptomycin (Life Technologies) in a humidified atmosphere with 10% CO_2 at 37°C. To differentiate cells, 100 ng/ml of NGF was added to the RPM 1640 medium with 0.1% HS, 0.05% FBS, 50 unit/ml penicillin, and 100 µg/ml streptomycin for 4 days.

Transfection

Plasmids used for transfection were constructed using pIRES-EYFP vector (Clontech, Nottinghamshire, UK). For electrophysiological recording, PC12 Tet-Off cells were transfected with mock, Flag-tagged wild-type or mutant (T415N) parkin cDNA, using Lipofectamine 2000. The engineered PC12 cells are constructed to have higher transfection efficiency than wild-type PC12 cells (unpublished data). After 24 h of transfection, cells were treated with NGF and differentiated for 4–5 days. More precisely, 3.0×10^5 cells were seeded in 35-mm dishes in RPMI with 10% HS and 5% FBS. Twenty-four hours after seeding, the medium was replaced with 500 µl of serum-free RPMI 1640 medium. Then, the transfection mixture containing 4 µg of cDNA and 10 µl of Lipofectamine 2000 in 500 µl of RPMI-1640 was added to each dish and incubated for 6 h in a humidified atmosphere with 10% CO_2 at 37°C. One milliliter of complete RPMI-1640 supplemented with an additional 10% HS and 5% FBS was then added to each dish. The solution for transfection was discarded 18 h later and replaced with RPMI-1640 medium for differentiation with added 100 ng/ml NGF. For transfection of α-synuclein, plasmids were constructed using pIRES-EGFP vector (Clontech) and the same protocol was used as for parkin. For protein analysis, cells (7.5×10^5/well, Clontech) were transfected in the same way. After 24 h, cells were subjected to Western blot analysis.

Western blot analysis

After 48 h of transfection of pIRES-EYFP-mock, pIRES-EYFP-Flag-wild-type parkin, or -T415N parkin with Lipofec-

tamine 2000 (Invitrogen), cells were lysed with TBS buffer (25 mM Tris/150 mM NaCl, PH 7.4) containing 1% Triton X-100 and centrifuged at 15,000 rpm for 30 min at 4°C. Thirty micrograms of each protein was subjected to SDS–PAGE on a 15% gel and transferred to PVDF membranes (Bio Rad, CA) and immunoblotted with anti-Flag M2 (1:200, Sigma, monoclonal) or anti-Actin (1:200, Chemicon, Temecula, CA, monoclonal).

Immunocytochemical analysis

After transfection, cells were fixed with 4% paraformaldehyde. Immunocytochemistry on PC12 Tet-Off cells was performed as previously described (Osaka et al., 2003) using antibodies against parkin (5 µg/ml, Zymed, San Francisco, CA; monoclonal), $P2X_2$, $P2X_4$, or $P2X_6$ receptor (1:200, Alomone labs, Jerusalem, Israel; polyclonal), ubiquitin that is predominantly reactive to free ubiquitin in immunohistochemistry (1:100, Sigma; polyclonal), α-synuclein (1:500, BD Biosciences, San Jose, CA), and dopamine and cyclic AMP-regulated phosphoprotein (DARPP-32) (phosphor Thr-34 and phospho Thr-75) (1:500, Abcam, Cambridge, UK). For immunofluorescence studies, anti-rabbit IgG conjugated with Cy3 antibodies (1:200, Jackson Immuno Research, West Grove, PA) or Alexa Fluor 568 goat anti-mouse (1:250, Molecular Probes, Invitrogen) was used as secondary antibodies. The same strength of the laser wavelength or fluorescence was applied in the series of images, for the quantification of the fluorescence under the confocal laser microscope system (LSM510, Carl Zeiss, Oberkochen, Germany).

Electrophysiological measurements

Cells expressing EYFP were selected under the fluorescence microscope. A patch pipette was then applied to the cell to obtain a giga-ohm seal under phase-bright mode. Whole-cell membrane current recordings were made under voltage-clamp at a holding potential of −70 mV as reported previously (Noda et al., 2000; Manago et al., 2005), using an Axopatch-200B amplifier (Axon Instruments, Foster City, CA). The patch pipette was filled with a solution containing (in mM): CsCl, 120; Mg_2ATP_3, 3; HEPES, 20; $CaCl_2$, 1; $MgCl_2$, 1; EGTA, 5. The pH of the solution was adjusted to 7.2 with 1 N CsOH. The pipette resistance was 5–9 MΩ. The external solution contained (mM): NaCl, 132; KCl, 5; $CaCl_2$, 2; $MgCl_2$, 1; glucose, 10; and HEPES, 10. The pH was adjusted to 7.4 with 1 N NaOH. External ATP or drugs were applied rapidly using the 'Y tube' technique (Min et al., 1996), which allows the complete exchange of the external solution surrounding a cell within 20 msec. Temperature monitored in the recording dishes was 33–34°C.

In the experiments with inhibitors (except PD98059), ATP was applied twice to ensure reproducibility of the ATP-induced current in control experiments. The inhibitor solution was applied after first application of ATP for a period appropriate to the inhibitor until the end of second application of ATP. The current amplitude obtained at the second application of ATP with or without inhibitors was normalized to that of the first ATP-induced current. All values were presented as mean ± SEM. Statistical analysis was done using ANOVA. A value of $P < 0.05$ was considered to be the minimum level of significance. Curve fitting was performed using the standard Hill Equation (Igor Pro 4.07; Wavemetrics, Lake Oswego, OR).

RESULTS
Transfection of parkin in PC12 Tet-Off cells

Expression of plasmid constructs was first examined in PC12 Tet-Off cells. Western blot analysis showed immunoreactive bands by anti-Flag antibodies in cells transfected with pIRES-EYFP-wild type parkin or T415N parkin, but not with mock plasmids (Fig. 1A). The efficiency of the transfection was about 10% in PC12 Tet-Off cells. To test endogenous expression of parkin, cells were immunostained using specific antibodies for parkin. The strong expression of parkin (red) was observed in wild-type parkin-transfected cell (yellow) but not in non-transfected cells in the same field (shown

A

mock   parkin^{WT} parkin^{T415N}

IB; anti-*Flag*

IB; anti-*Actin*

B

anti-Parkin   EYFP-Parkin

20 µm

C

mock   parkin^{WT} parkin^{T415N}
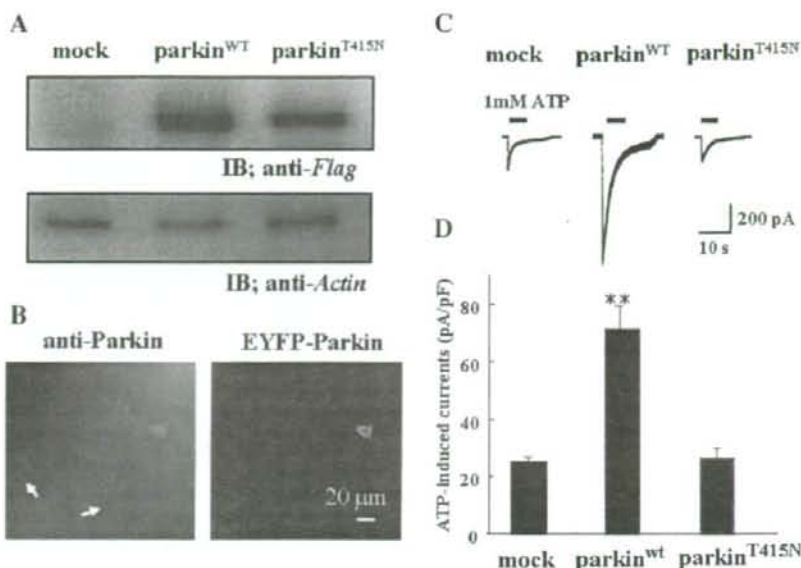
1mM ATP

200 pA

10 s

D

Fig. 1. Transfection of parkin and potentiation of ATP-induced currents in PC12 cells. **A:** Western blot analysis of PC12 Tet-Off cells. Cells were transfected with either pIRES-EYFP-mock, wild-type (WT) parkin, or T415N parkin. Each protein was subjected to SDS–PAGE and immunoblotted with anti-Flag or anti-Actin antibody. **B:** Confocal image of PC12 Tet-Off cells transfected with pIRES-EYFP-wild-type parkin (yellow) showed strong expression level of parkin (red) while non-transfected cells (white arrows) showed little expression of parkin. **C:** Inward membrane currents induced by 1 mM ATP at the holding potential of −70 mV in mock-, wild-type parkin-, and T415N parkin-transfected PC12 Tet-Off cells. **D:** Amplitudes of peak inward currents induced by 1 mM ATP in mock-, wild-type parkin-, and T415N parkin-transfected PC12 Tet-Off cells. The bars represent the mean ± SEM, **$P < 0.01$.

with white arrows in Fig. 1B), suggesting little endogenous parkin was expressed in PC12 Tet-Off cells.

Effects of expression of parkin on ATP-induced currents

ATP-activated inward currents due to the activation of P2X receptors at negative holding potentials in PC12 cells or PC12 Tet-Off cells have been reported previously (Nakazawa et al., 1994; Manago et al., 2005). In our experiments, PC12 Tet-Off cells were voltage-clamped at −70 mV and 1 mM ATP were applied to see whether or not overexpression of parkin affected maximum inward currents. In parkin-transfected cells, ATP-induced inward currents were nearly threefold larger than those in mock- or mutant (T415N) parkin-transfected cells (Fig. 1C). The amplitudes of the peak inward currents in mock-, wild-type parkin-, and T415N parkin-transfected PC12 Tet-Off cells were 24.8 ± 1.6 pA/pF (n = 9), 71.3 ± 8.4 pA/pF (n = 5), and 26.1 ± 3.4 pA/pF (n = 7), respectively (Fig. 1D).

The current–voltage relationships of the ATP-induced inward currents were determined by applying 50 msec voltage steps in 10 mV increments between −100 mV and +50 mV at 50 msec interval from the holding potential of −70 mV before and during the application of ATP (Fig. 2A). Current traces obtained before and after application of ATP in wild-type parkin-transfected cells are shown in Figure 2B. The current levels at the end of each pulse before and during ATP application were measured in mock-, wild-type parkin-, or T415N parkin-transfected cells. The amplitudes of the ATP-induced currents at each voltage were obtained by subtracting the one before application of ATP from the one during application of ATP. The current–voltage relationships obtained at the time point after 40 msec from the beginning of each pulse were plotted as in

Figure 2C. To allow for possible desensitization, the current–voltage relationships were also obtained by applying voltage steps in the opposite direction, that is, from +50 to −100 mV, but there was little change (data not shown). The reversal potential was about 0 mV, suggesting that these currents were due to non-specific cationic channels.

ATP-induced inward currents were concentration-dependent. Mock- and T415N parkin-transfected cells showed visible ATP-induced inward currents at 0.03 nM and a maximum response at 1 mM ATP (Fig. 3A). The maximum response was almost three times bigger in wild-type parkin-transfected cells (Fig. 3B). The sensitivity to ATP was not significantly changed by over-expression of either mock, wild-type, or T415N parkin. EC_{50} values (half maximum concentration) were 187 ± 45 µM, 127 ± 13 µM, and 177 ± 124 µM with Hill coefficients (n_H) of 1.05 ± 0.314, 0.97 ± 0.12, and 2.00 ± 2.26 in mock-, wild-type, and T415N parkin-transfected cells, respectively.

Expression of P2X$_2$, P2X$_4$, and P2X$_6$ receptors in parkin-transfected cells

In PC12 cells, P2X$_2$ and P2X$_4$ receptors (Hur et al., 2001) with lower level of P2X$_6$ receptor are expressed (our unpublished data). It was possible that the expression of P2X receptors was enhanced by overexpression of parkin. To define the changes in the expression level of P2X receptors semi-quantitatively, P2X$_2$, P2X$_4$, and P2X$_6$ receptors were immunostained using specific antibodies for each receptor subtype. The subcellular localization of P2X$_2$, P2X$_4$, and P2X$_6$ receptors showed no obvious difference in wild-type parkin-transfected cells compared with non-transfected cells in the same field (Fig. 4), suggesting that the potentiation of the
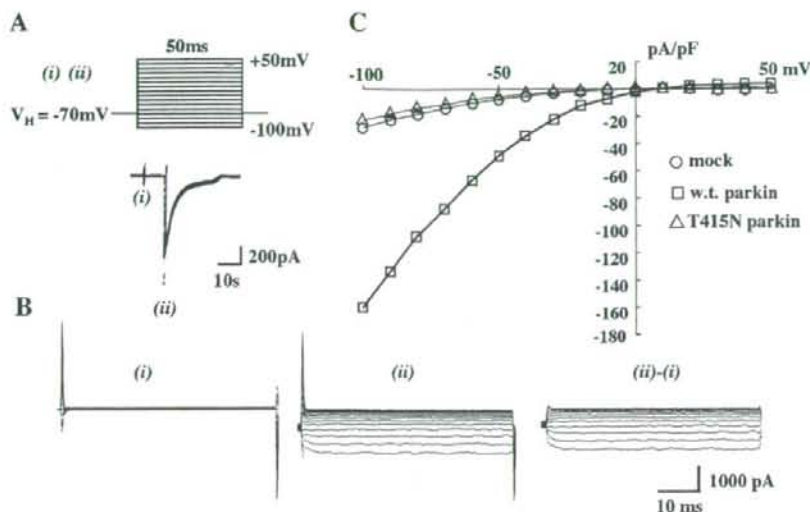
Fig. 2. Voltage-dependency of ATP-induced currents in mock-, wild-type parkin-, and T415N parkin-transfected PC12 Tet-Off cells. A: The voltage protocol shown in the upper part was applied before and during application of 1 mM ATP at the time indicated by (i) and (ii) in the lower part. B: Cumulated current traces obtained in wild-type parkin-transfected cells before (i) and during (ii) application of ATP.

The subtracted currents [(ii) − (i)] show the ATP-induced currents. C: The current–voltage relationships of ATP-induced currents. The amplitudes of subtracted currents [(ii) − (i)] in (B) at the end of 50 msec pulses were plotted against the pulse potentials in mock (○)-, wild-type (w.t.) parkin (□)-, and T415N parkin (△)-transfected cells.

ATP-induced currents was not due to an increase in the total number of P2X receptors.

Expression of mono-ubiquitin in parkin-transfected cells

It has previously been reported that a de-ubiquitinating isozyme, ubiquitin carboxy-terminal hydrolase L1 (UCH-L1), also potentiated ATP-induced currents (Manago et al., 2005). However, hydrolase activity was not involved in the potentiation of ATP-induced currents because a mutant form lacking hydrolase activity also potentiated the current. Instead, UCH-L1 upregulated ubiquitin levels (Osaka et al., 2003) and overexpression of UCH-L1 in PC12 cells increased the mono-

ubiquitin level (Manago et al., 2005). To test whether or not parkin also upregulate mono-ubiquitin levels, ubiquitin was stained using anti-mono-ubiquitin IgG. Unlike the effect of UCH-L1, immunoreactivity for ubiquitin in wild-type parkin-transfected cells was unchanged compared to that in mock-transfected cells or non-transfected cells in the same field (Fig. 5). These results indicated that parkin did not upregulate mono-ubiquitin.

Little effects of α-synuclein on ATP-induced currents

Since it has recently been shown that UCH-L1, parkin, and α-synuclein form lysine 63-linked multi-ubiquitin chains (Doss-Pepe et al., 2005; Lim et al.,
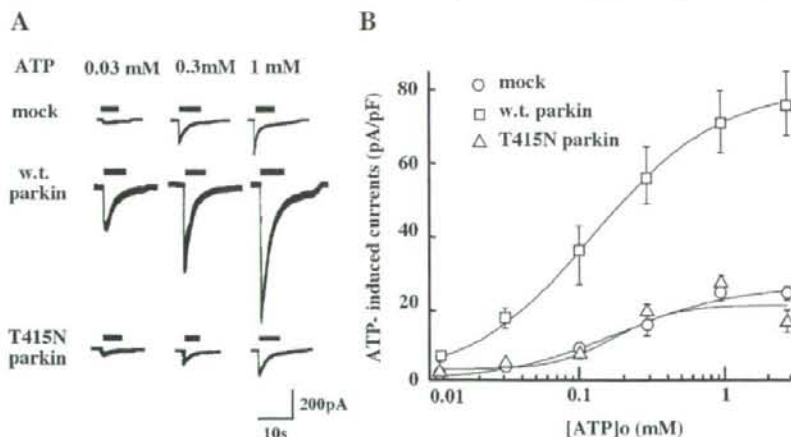

Fig. 3. Concentration-dependent curve of ATP-induced currents in mock-, wild-type parkin-, and T415N parkin-transfected PC12 Tet-Off cells. A: Inward membrane currents induced by 0.03, 0.1, and 1 mM ATP at the holding potential of −70 mV in mock-, wild-type (w.t.) parkin-, and T415N parkin-transfected PC12 Tet-Off cells. B: The peak inward current induced by ATP at the holding potential of

−70 mV was plotted against the ATP concentration at several points between 0.01 and 3 mM in mock (○)-, wild-type parkin (□)-, and T415N parkin (△)-transfected PC12 Tet-Off cells. Each point represents the mean of 5–13 cells and the bar shows the mean ± SEM. The curve shows the least squares fit.
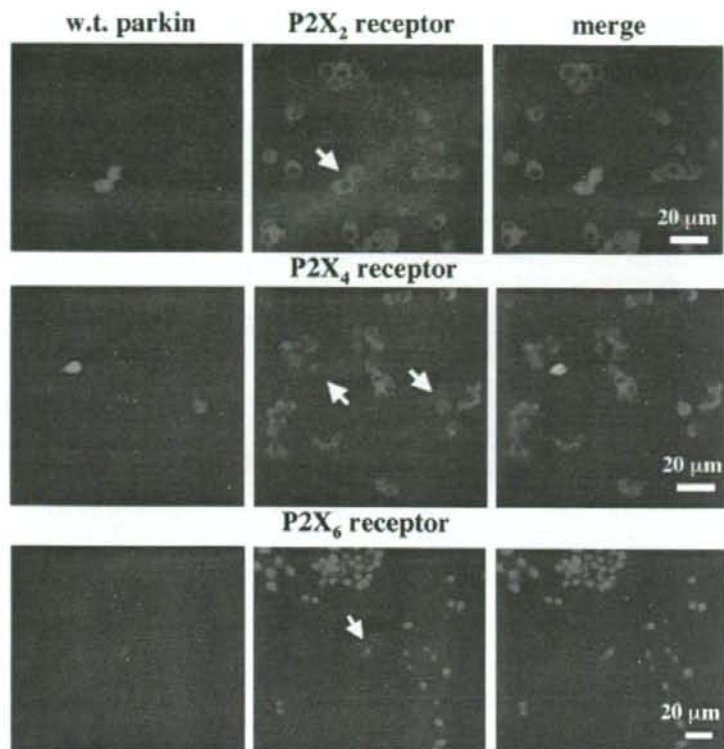
SATO ET AL.

| w.t. parkin | P2X$_2$ receptor | merge |

Fig. 4. Parkin has no clear effect on the expression of P2X$_2$, P2X$_4$, and P2X$_6$ receptors. Confocal images of PC12 Tet-Off cells transfected with pIRES-EYFP-wild-type (w.t.) parkin that were double stained with P2X$_2$ (**upper part**), P2X$_4$ (**middle part**), and P2X$_6$ receptors (**lower part**). EYFP (yellow)-positive cells were parkin-transfected cells, showing similar expression level of P2X receptors (red) to those in non-transfected cells.

2005), α-synuclein also might have a similar effect on P2X receptor. Transfection of α-synuclein was performed in the same way as parkin and the transfection efficiency was much greater than that of parkin (up to 30%) and the protein expression was confirmed by Western blotting (not shown). The strong expression of α-synuclein (red) was observed in transfected cell (green) but not in non-transfected cells in the same field
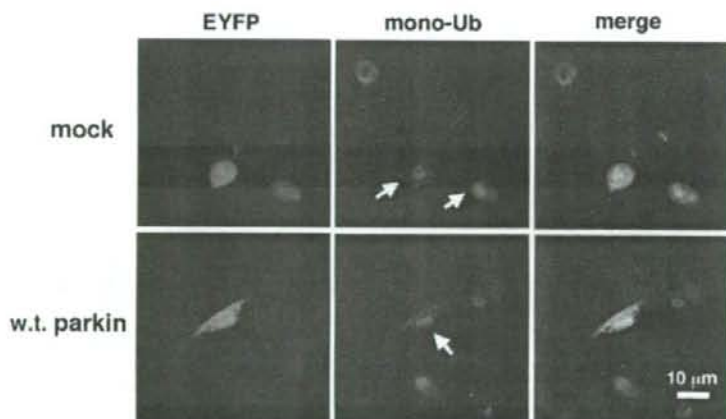

Fig. 5. Parkin had no clear effect on mono-ubiquitin expression. Confocal images of PC12 cells transfected with pIRES-mock or wild-type (w.t.) parkin that were double stained with mono-ubiquitin (red) and EYFP (yellow).

(shown with white arrows in Fig. 6A), suggesting little endogenous α-synuclein was expressed in PC12 Tet-Off cells.

ATP-induced currents in α-synuclein-transfected cells were not significantly different from those in mock-transfected cells (Fig. 6B). The relative amplitude of ATP-induced currents were 28.6 ± 4.1 pA/pF (n = 9) in mock-transfected cells and 21.5 ± 5.4 pA/pF (n = 10) in α-synuclein-transfected cells, respectively.

Effects of kinase inhibitors on ATP-induced currents in parkin-transfected cells

The mechanism by which ATP-induced currents were augmented in parkin-transfected cells was investigated. It was reported that in *Aplysia* UCH activated PKA as a result of degradation of the regulatory subunit of PKA, and that this contributed to the long-term potentiation (Hegde et al., 1997). The increase of the ATP-induced inward currents in UCH-L1-transfected cells has also been attributed to activation of PKA (Manago et al., 2005). Therefore, it was tested whether PKA might be activated in parkin-transfected cells by using H-89, a PKA inhibitor. After obtaining large ATP-induced currents in parkin-transfected cells, 10 μM H-89 was applied for 10 min. The amplitude of the ATP-induced currents in the presence of H-89 was 64.6 ± 3.5% (n = 7) of that of the first ATP-induced current in the same cell (control without H-89; 85.3 ± 4.0% (n = 4)) (Fig. 7A), implying an inhibition of about 25%. An inactive analog of H-89, H-85, did not have this inhibitory effect (current amplitude in the presence of H-85 was 84.3 ± 1.6% (n = 3) of the first current). To confirm the effect of parkin, the effect of PKA inhibitor on ATP-induced currents were tested in mock-transfected cells as well. In mock-transfected cells, application of 10 μM H-89 for 10 min had no effect on the ATP-induced inward current (H-89, 79.8 ± 1.4% (n = 3); control; 77.6 ± 5.2% (n = 3)) (Fig. 7B).

The intracellular carboxyl terminus of P2X receptor contains several consensus phosphorylation sites for protein kinase C (PKC) as well as PKA, suggesting that the function of the P2X receptors might be regulated by PKC-mediated phosphorylation (Chow and Wang, 1998). Hence, the effect of chelerythrine, a PKC inhibitor, on ATP-induced currents in parkin-transfected

cells was tested. Application of 5 μM chelerythrine for 10 min had no effect on the ATP-induced inward current in wild-type parkin-transfected cells (Fig. 7A). The normalized amplitude of second ATP-induced inward currents in the presence of chelerythrine was 88.4 ± 3.3% (n = 5). The possible involvement of calmodulin-dependent protein kinase (CaMKII) was also tested by using KN-93, a CaMKII inhibitor. Application of 10 μM KN-93 for 20 min had no effect on the ATP-induced inward current in wild-type parkin-transfected cell (90.4 ± 5.1% (n = 4); control, 81.2 ± 4.6% (n = 4)) (Fig. 7C).

In PC12 cells and hippocampal neurons, activation of PKA has been reported to cause activation of extracellular signal-regulated kinase (ERK), with subsequent phosphorylation of Ca^{2+}-stimulated cAMP response element binding protein (CREB) and stimulated transcription (Impey et al., 1998). Likewise, the augmentation of ATP response in parkin-transfected cell might be due to the stimulation of transcription. To test this possibility, we examined whether mitogen-activated protein kinase (MAPK), including ERK, was activated following the activation of PKA in PC12 Tet-Off cells. However, ATP-induced currents in parkin-transfected cells were unaffected even after application of 5 μM PD98059, (one of the MAPK kinase inhibitors) for 4 days: the amplitude of the ATP-induced current after the application of PD98059 was 82.1 ± 9.9 pA/pF (n = 4) compared with 74.6 ± 3.4 pA/pF (n = 18) in controls treated with vehicle (Fig. 7D).

Involvement of DARPP-32 in parkin-transfected PC12 Tet-Off cells

It was previously reported that the dopamine and cAMP-regulated phosphoprotein with molecular weight of about 32,000 (DARPP-32) was expressed in PC12 Tet-Off cells and that the expression level tended to increase after differentiation of the cells with NGF (Manago et al., 2005). Since phosphorylation of DARPP-32 at Thr-75 by cyclin-dependent kinase 5 (CDK5) had a negative feedback regulatory effect on PKA activity (Nishi et al., 2000), the effect of roscovitine, a CDK5 inhibitor, was tested. The application of 10 μM roscovitine to wild-type parkin-expressing cells for 10 min enhanced the normalized amplitude of ATP-induced currents to the one
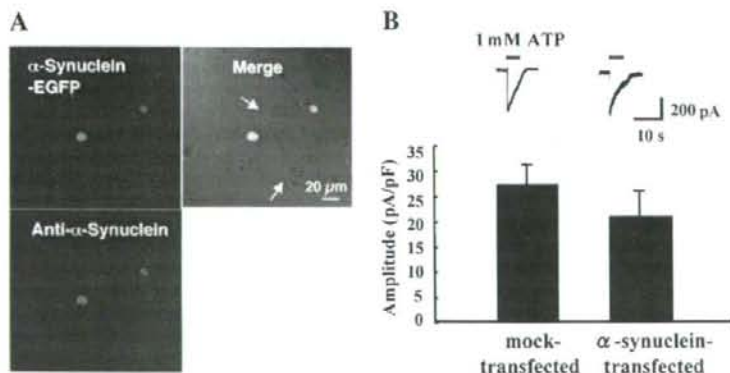

Fig. 6. The wild-type α-synuclein-transfection had no effect on ATP-induced currents. **A:** α-synuclein-transfected cells (EGFP; green) were strongly stained with anti-α-synuclein (red), while non-transfected cells (with arrows) were not. **B:** The amplitude of ATP-induced inward currents in mock and α-synuclein-transfected cells.
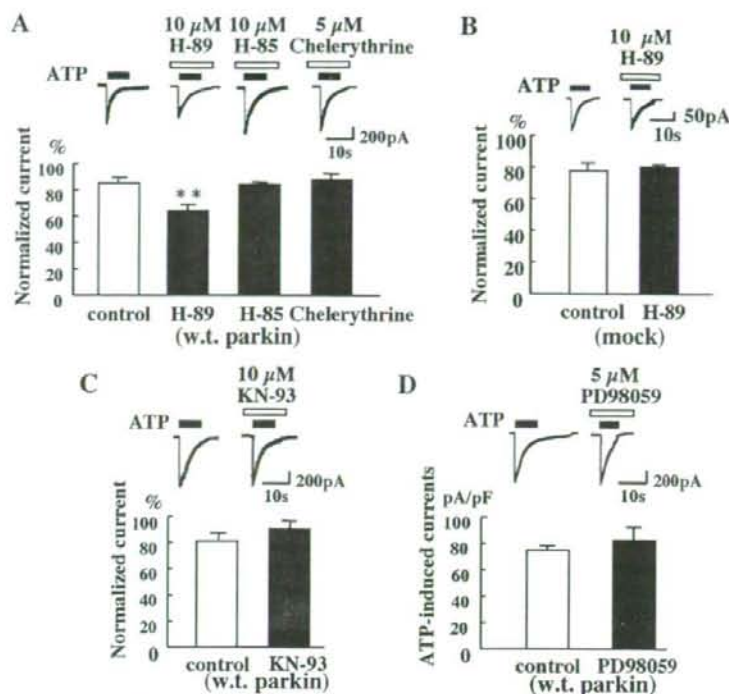
SATO ET AL.

Fig. 7. Effects of kinase inhibitors on ATP-induced currents. A: In wild-type parkin-transfected cells, ATP-induced currents were attenuated by pre-application of 10 μM H-89, a PKA inhibitor, but not either by 10 μM H-85, an inactive analog of H-89, or 5 μM chelerythrine, a PKC inhibitor, for 10 min. B: H-89 had no effect on ATP-currents in control (mock-transfected) cells. C, D: In wild-type parkin-transfected cells, ATP-induced currents were not affected by application of 10 μM KN-93, a CaMKII inhibitor, for 20 min (C), or by treatment with 5 μM PD98059, a MAPKK inhibitor, for 4 days during differentiation (D). **$P < 0.01$.

before application of roscovitine ($102.1 \pm 3.5\%$ (n = 4); control without roscovitine; $85.3 \pm 4.0\%$ (n = 4)) (Fig. 8A). The result suggested that PKA activity in parkin-transfected cells was negatively regulated by the phosphorylation of DARPP-32 at Thr-75 by CDK5.

Activation of PKA also influenced on protein phosphatases relating to DARPP-32 (Nishi et al., 2000). The phosphorylation of DARPP-32 at Thr-34 has been reported to inhibit protein phosphatase-1 (PP-1), leading to an apparent increase in substrate-phosphorylation. On the other hand, PKA activates protein phosphatase-2A (PP-2A), causing dephosphorylation of DARPP-32 at Thr-75, activating PKA in turn. To investigate the role of PP-1 and PP-2A in parkin-transfected cells, we applied 100 nM okadaic acid, an inhibitor for both PP-1 and PP-2A, for 20 min. The normalized currents were augmented to $98.7 \pm 4.5\%$ (n = 5) (control without okadaic acid; $81.2 \pm 4.6\%$ (n = 4) (Fig. 8B). These results suggested that the function of PP-1 was superior to that of PP-2A in parkin-transfected cells.

The effects of CDK5 inhibitor and okadaic acid on ATP-induced currents were tested in mock-transfected cells as well. In mock-transfected cells, application of 10 μM roscovitine for 10 min had no effect on the ATP-induced inward current (roscovitine, $82.5 \pm 5.2\%$ (n = 3); control; $77.6 \pm 5.2\%$ (n = 3)) (Fig. 8C). Similarly, application of 100 nM okadaic acid for 20 min did not affect the ATP-induced currents in mock-transfected cells, ($76.5 \pm 3.5\%$ (n = 3); control; $80.0 \pm 4.7\%$ (n = 3)) (Fig. 8D).

Phosphorylation of DARPP-32 in parkin-transfected PC12 Tet-Off cells

To investigate whether or not the phosphorylation of DARPP-32 at Thr-34 or Thr-75 was modified by parkin, cells were immunostained using specific antibodies for DARPP-32 (phospho Thr-34 or phospho Thr-75). The staining of phospho Thr-34 in parkin-transfected cells were not enhanced as expected from the activation of PKA (Nishi et al., 2000) but rather attenuated (Fig. 9A). While phospho Thr-75 looked similar between parkin-transfected cell and non-transfected cells in the same field (Fig. 9B).

DISCUSSION

To understand the functional role of parkin in the central nervous system (CNS), it is important to know whether parkin has any effects on ion channels and receptors that are the basic elements of neurotransmission. To test this, we used PC12 cells and overexpressed parkin protein (Fig. 1A). These show well-developed inward current response to stimulation of P2X receptors by ATP (Nakazawa et al., 1994) and we recently reported enhancement of these currents by ubiquitin C-terminal hydrolase L1 (UCH-L1) (Manago et al., 2005). In the present experiments, we have studied the effects of overexpressing of parkin on these currents.

Parkin produced a very substantial increase in the maximum ATP-induced current without significant change in sensitivity to ATP (Figs. 1 and 3). This did not appear to be due to an increased number of P2X$_2$,
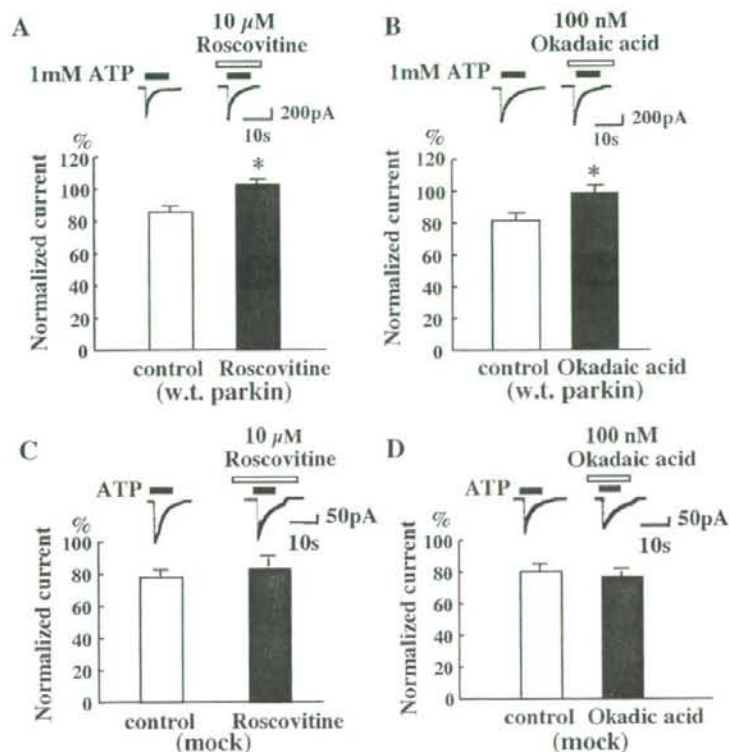
Fig. 8. Involvement of DARPP-32-relating protein kinase and protein phosphatase on ATP-induced currents. In wild-type parkin-transfected cells, ATP-induced currents were augmented by pre-application of roscovitine, a CDK5 inhibitor, for 10 min (A) or 100 nM okadaic acid, a protein phosphatase inhibitor, for 20 min (B). In mock-transfected cells, ATP-induced currents were not affected by 10 μM roscovitine (C) or 100 nM okadaic acid (D). **$P < 0.05$.

Fig. 9. Parkin did not increase the phosphorylation of DARPP-32. A: Immunostaining of phospho Thr-34 (red) looked rather smaller in parkin-transfected cell (yellow-green; white arrow). B: Immunostaining of phospho Thr-75 (red) looked similar between parkin-transfected cell (white arrow) and non-transfected cells. The merged images also include differential interference contrast images.

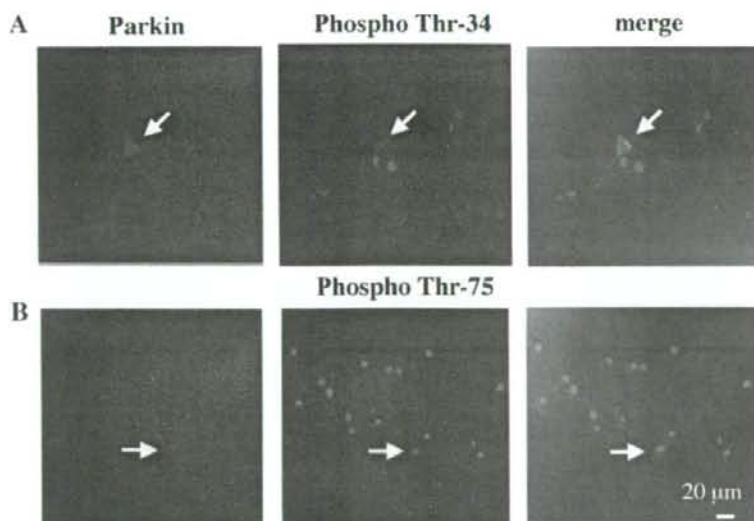P2X$_4$, or P2X$_6$ receptors, as judged by immunocyto-chemistry (Fig. 4). Therefore, the mechanism seems to involve an increase in gating of the receptors, rather than increased affinity or receptor number. Enhancement of P2X receptor at presynaptic terminal could increase neurotransmitter release; it was reported that ischemia-induced facilitation of glutamate release was due to the activation of P2X receptors in spiny neuron in neostriatum (Zhang et al., 2006) and our preliminary result showed that ATP increased the frequency of miniature inhibitory postsynaptic potential (mIPSP) in acutely isolated neuron from substantia nigra, suggesting increased release of GABA from presynaptic terminal (unpublished data).

The enhancement of ATP-induced currents seemed to be associated with the ubiquitin ligase activity of parkin since it was not reproduced by a ligase-deficient mutant (Figs. 2C and 3). Involvement of the ubiquitin–proteasome system would accord with our previous observations with the ubiquitin hydrolase UCH-LI, though in this case hydrolase activity itself was not required since the effect of UCH-LI was replicated by a hydrolase-deficient construct. Instead, upregulation of mono-ubiquitin (Osaka et al., 2003) and ubiquitin ligase activity of UCH-L1 (Liu et al., 2002) might be responsible for the potentiation of ATP-induced currents.

Though the precise mechanism how ubiquitin ligase activity of parkin is involved is not known yet, possible signaling leading to enhancement of the ATP-induced currents is summarized in Fig. 10. It is only a part of the mechanism revealed in the present investigation, because inhibition of PKA, CDK5 or phosphatases resulted in only partial (±20%) inhibition of the parkin-potentiated currents which showed threefold increase in amplitude compared to control.

At least, part of the increase in ATP-induced currents appeared to result from activation of PKA directly or indirectly, because PKA inhibitor partially attenuated parkin-induced potentiaion of ATP-currents (Fig. 7A). In a reverse way, activation of PKA by forskolin augmented the ATP-induced currents in mock-transfected cells (Manago et al., 2005). One possible mechanism would be phosphorylation of P2X receptors by PKA. It was reported that activation of PKA potentiated ATP-evoked current in P2X$_4$-transfected HEK293 cells (Brown et al., 2004), while there was an opposite result in P2X$_2$-transfected HEK293 cells (Chow and Wang, 1998). CaMKII could be activated by PKA indirectly via an inhibition of PP-1 (Winder and Sweatt, 2001), but KN-93 did not have any effect on ATP-induced currents in parkin-transfected cells (Fig. 7C), suggesting that CaMKII was not significantly activated by parkin.

Since the enhancement was not completely reversed by inhibition of PKA, other mechanisms must be involved. One such mechanism might be through modification of DARPP-32. In rat striatum, it has been suggested that there is positive and negative feedback regulation of DARPP-32 via activation of PKA and CDK5, respectively (Nishi et al., 2000). Since DARPP-32 was expressed in PC12 cells (Manago et al., 2005), its possible involvement was tested using roscovitine, a CDK5 inhibitor, and okadaic acid, a protein phosphatase (PP-1 and PP-2A) inhibitor. Roscovitine further enhanced the ATP-induced currents in parkin-transfected cells (Fig. 8A), suggesting a negative-feedback role for CDK5. It seemed likely that parkin stimulated CDK5 since roscovitine did not have significant effect on mock-transfected cells (Fig. 8C). On the other hand, a role for phosphatases was suggested by the fact that okadaic acid further enhanced the ATP-induced
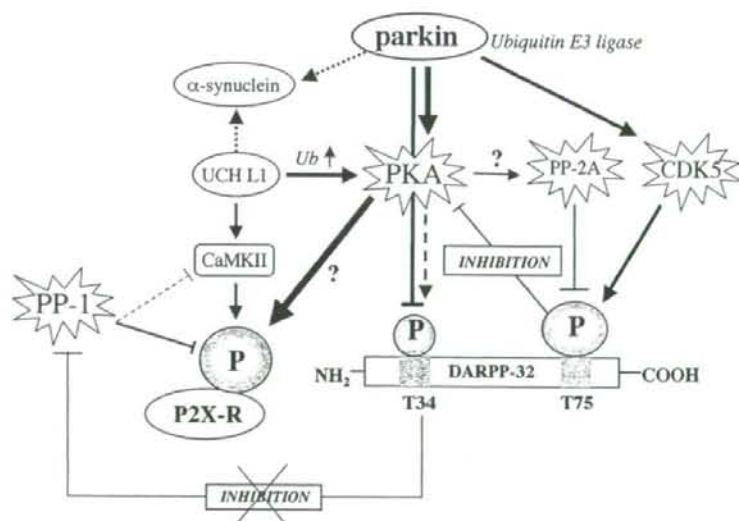

Fig. 10. Predicted signaling induced by expression of parkin. Parkin may activate PKA, subsequently phosphorylating P2X receptors. Parkin also may activate protein phosphatase-1 (PP-1) via inhibiting phosphorylation of DARPP-32 at Thr-34. On the other hand, phosphorylation and dephosphorylation of DARPP-32 at Thr-75 by CDK5 and PP-2A could compete with each other, keeping the level of phospho Thr-75 unchanged. As additional information, ubiquitin C-terminal hydrolase (UCH-L1) also activates PKA, which is independent on hydrolase activity but presumably due to the increase in mono-ubiquitin level (Manago et al., 2005) or ubiquitin ligase activity (Liu et al., 2002). Unlike parkin, UCH-L1 activates Ca^{2+} and calmodulin-dependent protein kinase (CaMKII), which could be indirectly activated by PKA and dephosphorylated by PP-1 (Winder and Sweatt, 2001). The effect of α-synuclein, a substrate for both parkin and UCH-L1 (dotted line), was not clear, because transfection of α-synuclein did not affect ATP-induced currents. Reported signaling but not confirmed in the present study was shown by dotted line.

currents in parkin-transfected cells (Fig. 8B). Since inhibition of PP-2A was supposed to inhibit PKA activity (Nishi et al., 2000; Manago et al., 2005), it seemed likely that this enhancement resulted mainly from inhibition of PP-1. In mock-transfected cells, okadaic acid did not have significant effect (Fig. 8D).

As for the phosphorylation of DARPP-32, activation of PKA would phosphorylate DARPP-32 at Thr-34 (Nishi et al., 2000). However, the staining of phospho Thr-34 was rather attenuated in parkin-transfected cells (Fig. 9A), suggesting that parkin may have inhibitory effect on the phosphorylation site at Thr-34. Therefore, parkin might indirectly activate PP-1, canceling the negative feedback from phospho Thr-34. Concerning the phosphorylation of DARPP-32 at Thr-75, CDK5, and PP-2A were supposed to have opposite effects, keeping the same level of phospho Thr-75 (Fig. 9B).

Both UCH-L1 and parkin can operate via α-synuclein as a target substrate (Shimura et al., 2001; Snyder and Wolozin, 2004). It has recently been shown that UCH-L1, parkin, and α-synuclein form lysine 63-linked multiubiquitin chains, which induce proteasomal-independent ubiquitination (Doss-Pepe et al., 2005; Lim et al., 2005). Therefore, it was possible that α-synuclein also had potentiating effect on P2X receptors if lysine 63-linked multiubiquitin was involved. However, α-synuclein did not have such effect (Fig. 6). It will be great interest to investigate the relationship between these three proteins and it may help to understand why parkin deficient-mice are not a robust model of parkinsonism (Perez and Palmiter, 2005), though there were alterations in energy metabolism, protein handling, and synaptic function (Periquet et al., 2005).

Another interesting point is that the signaling between activation of PKA and potentiation of P2X receptors induced by either UCH-L1 or parkin was not the same. For example, UCH-L1 but not parkin activated CaMKII and PP-2A whereas parkin but not UCH-L1 seemed to activate CDK5, providing a negative feedback effect on PKA (Fig. 10). In addition, we found that DARPP-32 (phospho Thr-34) was rather attenuated in spite of the report that activation of PKA increased the phosphorylation at Thr-34 (Nishi et al., 2000). The difference between UCH-L1 and parkin might due to the different substrate specificity as ubiquitin ligases.

Unfortunately, the low transfection efficiency precluded direct biochemical studies on the phosphorylation or dephosphorylation of specific proteins by parkin or UCH-L1. As a result, we have been restricted to pharmacological and immunocytochemical analyses. Nevertheless, the important point we have established is that enzymes working in the ubiquitin–proteasome system have clear and substantial effects on a neurotrasmitter receptor and hence subsequently may affect neurotransmission in vivo. It is widely accepted that there are number of diseases related to aberrations in the ubiquitin system (Ciechanover and Schwartz, 2004), but how aberrations in the ubiquitin system cause neurodegenrative diseases such as Parkinson's disease (PD) is largely unknown. In the present study, one of the ubiquitin ligases, parkin, potentiated the function of P2X receptors, as well as another enzyme working in the ubiquitin–proteasome system, UCH-L1. Presynaptic P2X receptors triggers Ca^{2+}-dependent glutamate release in the brainstem (Shigetomi and Kato, 2004), though ATP-mediated inhibition of dopamine release was reported in rat neostriatum (Trendelenburg and Bultmann, 2000). It is of great interest how endogenous

parkin or UCH-L1 modulates neurotransmitter release by stimulating P2X receptors in vivo, which is now under investigation.

LITERATURE CITED

Brown DA, Bruce JI, Straub SV, Yule DI. 2004. cAMP potentiates ATP-evoked calcium signaling in human parotid acinar cells. J Biol Chem 279:39485–39494.
Chow YW, Wang HL. 1998. Functional modulation of P2X2 receptors by cyclic AMP-dependent protein kinase. J Neurochem 70:2606–2612.
Ciechanover A, Schwartz AL. 2004. The ubiquitin system: Pathogenesis of human diseases and drug targeting. Biochim Biophys Acta 1695:3–17.
Cookson MR. 2005. The biochemistry of Parkinson's disease. Annu Rev Biochem 74:29–52.
Doss-Pepe EW, Chen L, Madura K. 2005. Alpha-synuclein and parkin contribute to the assembly of ubiquitin lysine63-linked multiubiquitin chains. J Biol Chem 280:16619–16624.
Hegde AN, Inokuchi K, Pei W, Casadio A, Ghirardi M, Chain DG, Martin KC, Kandel ER, Schwartz JH. 1997. Ubiquitin C-terminal hydrolase is an immediate-early gene essential for long-term facilitation in Aplysia. Cell 89:115–126.
Hur EM, Park TJ, Kim KT. 2001. Coupling of L-type voltage-sensitive calcium channels to P2X(2) purinoceptors in PC-12 cells. Am J Physiol Cell Physiol 280:C1121–C1129.
Huynh DP, Scoles DR, Nguyen D, Pulst SM. 2003. The autosomal recessive juvenile Parkinson disease gene product, parkin, interacts with and ubiquitinates synaptotagmin XI. Hum Mol Genet 12:2587–2597.
Imai Y, Soda M, Takahashi R. 2000. Parkin suppresses unfolded protein stress-induced cell death through its E3 ubiquitin-protein ligase activity. J Biol Chem 275:35661–35664.
Impey S, Obrietan K, Wong ST, Poser S, Yano S, Wayman G, Deloulme JC, Chan G, Storm DR. 1998. Cross talk between ERK and PKA is required for Ca^{2+} stimulation of CREB-dependent transcription and ERK nuclear translocation. Neuron 21:869–883.
Kitada T, Asakawa S, Hattori N, Matsumine H, Yamamura Y, Minoshima S, Yokochi M, Mizuno Y, Shimizu N. 1998. Mutations in the parkin gene cause autosomal ecessive juvenile parkinsonism. Nature 392:605–608.
Ko HS, von Coelln R, Sriram SR, Kim SW, Chung KK, Pietnikova O, Troncoso J, Johnson B, Saffary R, Goh EL, Song H, Park BJ, Kim MJ, Kim S, Dawson VL, Dawson TM. 2005. Accumulation of the authentic parkin substrate aminoacyl-tRNA synthetase cofactor, p38/JTV-1, leads to catecholaminergic cell death. J Neurosci 25:7968–7978.
Kubo S, Kitami T, Noda S, Shimura H, Uchiyama Y, Asakawa S, Minoshima S, Shimizu N, Mizuno Y, Hattori N. 2001. Parkin is associated with cellular vesicles. J Neurochem 78:42–54.
Lim KL, Chew KC, Tan JM, Wang C, Chung KK, Zhang Y, Tanaka Y, Smith W, Engelender S, Ross CA, Dawson VL, Dawson TM. 2005. Parkin mediates nonclassical, proteasomal-independent ubiquitination of Synphilin-1: Implications for Lewy body formation. J Neurosci 25:2002–2009.
Liu Y, Fallon L, Lashuel HA, Liu Z, Lansbury PT Jr. 2002. The UCH-L1 gene encodes two opposing enzymatic activities that affect alpha-synuclein degradation and Parkinson's disease susceptibility. Cell 111:209–218.
Manago Y, Kanahori Y, Shimada A, Sato A, Amano T, Sato-Sano Y, Setsuie R, Sakurai M, Aoki S, Wang YL, Osaka H, Wada K, Noda M. 2005. Potentiation of ATP-induced currents due to the activation of P2X receptors by ubiquityin carboxy-terminal hydrolase L1. J Neurochem 92:1061–1072.
Min BI, Kim CJ, Rhee JS, Akaike N. 1996. Modulation of glycin-induced chloride current in acutely dissociated rat periaqueductal gray neurons by l-opioid agonist DAGO. Brain Res 734:72–78.
Nakazawa K, Inoue K. 1992. Roles of Ca^{2+} influx through ATP-activated channels in catecholamine release from pheochromocytoma PC12 cells. J Neurophysiol 68:2026–2032.
Nakazawa K, Inoue K, Koizumi S, Inoue K. 1994. Facilitation by 5-hydroxytryptamine of ATP-activated current in rat pheochromocytoma cells. Pflügers Arch 427:492–499.
Nishi A, Bibb JA, Snyder GL, Higashi H, Nairn AC, Greengard P. 2000. Amplification of dopaminergic signaling by a positive feedback loop. Proc Natl Acad Sci USA 97:12840–12845.
Noda M, Nakanishi H, Nabekura J, Akaike N. 2000. AMPA-kainate subtypes of glutamate receptor in rat cerebral microglia. J Neurosci 20:251–258.
Osaka H, Wang YL, Takada K, Takizawa S, Setsuie R, Li H, Sato Y, Nishikawa K, Sun YJ, Sakurai M, Harada T, Hara Y, Kimura I, Chiba S, Namikawa K, Kiyama H, Noda M, Aoki S, Wada K. 2003. Ubiquitin carboxy-terminal

hydrolase L1 binds to and stabilizes monoubiquitin in neuron. Hum Mol Genet 12:1945–1958.

Perez FA, Palmiter RD. 2005. Parkin-deficient mice are not a robust model of parkinsonism. Proc Natl Acad Sci USA 102:2174–2179.

Periquet M, Corti O, Jacquier S, Brice A. 2005. Proteomic analysis of parkin knockout mice: Alterations in energy metabolism, protein handling and synaptic function. J Neurochem 95:1259–1276.

Sela D, Ram E, Atlas D. 1991. ATP receptor. A putative receptor-operated channel in PC-12 cells. J Biol Chem 266:17990–17994.

Shimura H, Hattori N, Kubo S, Mizuno Y, Asakawa S, Minoshima S, Shimizu N, Iwai K, Chiba T, Tanaka K, Suzuki T. 2000. Familial Parkinson disease gene product, parkin, is a ubiquitin-protein ligase. Nat Genet 25:302–305.

Shimura H, Schlossmacher MG, Hattori N, Frosch MP, Trockenbacher A, Schneider R, Mizuno Y, Kosik KS, Selkoe DJ. 2001. Ubiquitination of a new form of alpha-synuclein by parkin from human brain: Implications for Parkinson's disease. Science 293:263–269.

Snyder H, Wolozin B. 2004. Pathological proteins in Parkinson's disease: Focus on the proteasome. J Mol Neurosci 24:425–442.

Shigetomi E, Kato F. 2004. Action potential-independent release of glutamate by Ca^{2+} entry through presynaptic P2X receptors elicits postsynaptic firing in the brainstem autonomic network. J Neurosci 24:3125–3135.

Sriram SR, Li X, Ko HS, Chung KK, Wong E, Lim KL, Dawson VL, Dawson TM. 2005. Familial-associated mutations differentially disrupt the solubility, localization, binding and ubiquitination properties of parkin. Hum Mol Genet 14:2571–2586.

Trendelenburg AU, Bultmann R. 2000. P2 receptor-mediated inhibition of dopamine release in rat neostriatum. Neuroscience 96:249–252.

Winder DG, Sweatt JD. 2001. Roles of serine/threonine phosphatases in hippocampal synaptic plasticity. Nat Rev Neurosci 2:461–474.

Zhang Y, Gao J, Chung KK, Huang H, Dawson VL, Dawson TM. 2000. Parkin functions as an E2-dependent ubiquitin-protein ligase and promotes the degradation of the synaptic vesicle-associated protein, CDCrel-1. Proc Natl Acad Sci USA 97:13354–13359.

Zhang Y, Deng P, Li Y, Xu ZC. 2006. Enhancement of excitatory synaptic transmission in spiny neurons after transient forebrain ischemia. J Neurophysiol 95:1537–1544.

ARTICLE

Genomewide Association Analysis of Human Narcolepsy and a New Resistance Gene

Minae Kawashima, Gen Tamiya, Akira Oka, Hirohiko Hohjoh,* Takeo Juji, Takashi Ebisawa, Yutaka Honda, Hidetoshi Inoko, and Katsushi Tokunaga

Human narcolepsy is a hypersomnia that is affected by multiple genetic and environmental factors. One genetic factor strongly associated with narcolepsy is the *HLA-DRB1*1501-DQB1*0602* haplotype in the human leukocyte antigen region on chromosome 6, whereas the other genetic factors are not clear. To discover additional candidate regions for susceptibility or resistance to human narcolepsy, we performed a genomewide association study, using 23,244 microsatellite markers. Two rounds of screening with the use of pooled DNAs yielded 96 microsatellite markers (including 16 markers on chromosome 6) with significantly different estimated frequencies in case and control pools. Markers not located on chromosome 6 were evaluated by the individual typing of 95 cases and 95 controls; 30 markers still showed significant associations. A strong association was displayed by a marker on chromosome 21 (21q22.3). The surrounding region was subjected to high-density association mapping with 14 additional microsatellite markers and 74 SNPs. One microsatellite marker (*D21S0012m*) and two SNPs (*rs13048981* and *rs13046884*) showed strong associations ($P < .0005$; odds ratios 0.19–0.33). These polymorphisms were in a strong linkage disequilibrium, and no other polymorphism in the region showed a stronger association with narcolepsy. The region contains three predicted genes—*NLC1-A*, *NLC1-B*, and *NLC1-C*—tentatively named "narcolepsy candidate-region 1 genes," and *NLC1-A* and *NLC1-C* were expressed in human hypothalamus. Reporter-gene assays showed that the marker *D21S0012m* in the promoter region and the SNP *rs13046884* in the intron of *NLC1-A* significantly affected expression levels. Therefore, *NLC1-A* is considered to be a new resistance gene for human narcolepsy.

Narcolepsy (MIM 161400) typically appears, without sexual difference, in early adulthood and affects 0.16%–0.18% of the general population of Japan.[1,2] The disorder is characterized by excessive daytime sleepiness, cataplexy, and pathological manifestation of rapid eye movement (REM) sleep, including hypnagogic hallucinations, sleep paralysis, or sleep-onset REM sleep. Most cases are sporadic, but the risk of the disorder for first-degree relatives of patients with narcolepsy is 1%–2%, ~10 times greater than the general risk of developing narcolepsy. Only about a third of MZ twins are concordant for narcolepsy.[2] Therefore, human narcolepsy is considered to be a multifactorial disorder, involving multiple genetic and environmental factors.

A genetic susceptibility factor associated with the disorder has been found in the human leukocyte antigen (HLA) class II region: the *HLA-DRB1*1501-DQB1*0602* haplotype (*HLA-DRB1* [MIM 142857] and *HLA-DQB1* [MIM 604305]). Although almost all Japanese patients with narcolepsy carry this haplotype, ~10% of the general Japanese population also carries it, suggesting that this haplotype is neither necessary nor sufficient for the development of narcolepsy.[1,3-5] This conclusion is also supported by another line of reasoning. The penetrance and population frequency of *HLA-DRB1*1501* were estimated

with the formula described by Ohashi et al.,[8] based on the prevalence of narcolepsy in the Japanese population (0.16%–0.18%)[1,2] and the results of a case-control association study of this haplotype.[7] On the basis of these values and with the formula described by James[9] and by Risch,[10] the expected λs value for *HLA* of Japanese patients with narcolepsy was calculated to be 5.15, much less than the λs of 12 reported for narcolepsy.[6] Therefore, genes other than *HLA* are also expected to contribute to the disease susceptibility.

Several candidate regions[11-13] and genes[14,15] other than *HLA* have been investigated for association with human narcolepsy involving cataplexy (narcolepsy-cataplexy) and daytime sleepiness. Nevertheless, replicated associations are few, except for tumor necrosis factor-α (*TNFA* [MIM 191160]) and TNF-receptor 2 (*TNFR2* [MIM 191191]).[16-20] In autosomal recessive canine models that develop narcolepsy-cataplexy with full penetrance, an insertion in the hypocretin (orexin)–receptor type 2 gene (*HCRTR2* [MIM 602393]) was found to be responsible for the disorder,[21] and preprohypocretin-knockout mice exhibit a phenotype similar to narcolepsy-cataplexy.[22] For human narcolepsy, which shows multifactorial inheritance, as described above, the hypocretin concentration in cerebrospinal fluid was reduced or undetectable in spo-

radic narcolepsy,[23] and the number of hypothalamic hypocretin neurons was decreased in postmortem narcoleptic brains.[24,25] Although the preprohypocretin (MIM 602358) and hypocretin-receptor genes have been examined for possible association with human narcolepsy, variants in these genes were not detected in most human patients with narcolepsy.[26-28] Therefore, human narcolepsy cannot be explained by mutations in preprohypocretin and hypocretin-receptor genes.

There is evidence for a role of autoantibodies in narcolepsy. Recently, mice were injected with purified immunoglobulin G (IgG) fraction from the serum of nine patients who have narcolepsy-cataplexy with the HLA-DQB1*0602 haplotype. These mice exhibited stresslike behaviors, such as crouching posture and piloerection, and narcoleptic-like behavior, such as brief behavioral pauses lasting from a few seconds to a minute during periods of activity.[29] Another group revealed that IgG in the cerebrospinal fluid of HLA-DQB1*0602–positive patients with narcolepsy-cataplexy binds to rat hypothalamic proteins.[30] These two reports suggested that cerebrospinal fluid and serum from patients with narcolepsy contain functional autoantibodies that contribute to the pathogenesis of narcolepsy. However, the pathophysiological mechanism and genetic factors underlying human narcolepsy remain unknown.

For this study, we performed a genomewide association study, using 23,244 microsatellite markers for the detection of susceptibility/resistance regions to narcolepsy. This strategy is expected to be effective in the search for candidate regions throughout the whole genome, because of the high detection power of case-control association studies.[31,32] Microsatellite markers are abundant and interspersed throughout the human genome. Compared with SNPs, microsatellite markers display higher degrees of polymorphisms: multiple alleles exhibit high levels of heterozygosity, so a smaller number of microsatellite markers may provide a reasonable statistical power in association analyses.[33,34] Moreover, to reduce the genotyping cost and labor, genomic DNA samples were pooled[33,35] in the first and second screenings. We demonstrated elsewhere that this strategy can detect the known association with the HLA region; using 1,265 microsatellite markers on chromosome 6, we detected strong associations between multiple microsatellite markers in the HLA region and human narcolepsy.[36] Here, we extend the strategy to the other chromosomes, using 21,979 additional microsatellite markers.

Material and Methods
Patients and Unaffected Individuals

All patients and unaffected individuals were unrelated Japanese adults living in Tokyo or neighboring areas. Genomic DNAs were obtained from 370 patients given a diagnosis of narcolepsy-cataplexy at the Sleep Disorders Clinic of Seiwa Hospital. All patients with narcolepsy carried the HLA-DRB1*1501-DQB1*0602 haplotype. These 370 genomic DNAs were divided randomly into three

sets (the first and second sets with 110 samples each and the third set with the remaining 150 samples). The control group comprised 610 unrelated unaffected individuals and an additional 125 individuals positive for HLA-DRB1*1501. The 610 control samples were also divided into three sets (210 samples each in the first and second sets and the remaining 190 samples in the third set). Genomic DNAs were purified from peripheral blood, with the use of a commercial kit (QIAamp Blood Kit [Qiagen]). This study was approved by the research ethics review committees of the University of Tokyo and the Neuropsychiatric Research Institute, which runs Seiwa Hospital.

Preparation of Pooled DNA Samples

Genomic DNA concentration was measured in triplicate, in accordance with the methods of Collins et al.,[17] with the use of a double-stranded DNA quantification kit (PicoGreen [Molecular Probes]) with a microtiter plate reader (SF600 Corona Electric). Genomic DNAs were adjusted to 8 ng/μl. DNAs from 110 patients with narcolepsy and from 210 controls were then mixed, for the first set of case and control pools, named "case-1" and "control-1," respectively.[38] The second set of pooled DNA (case-2 and control-2) was also prepared from another 110 cases and 210 controls.

Analyses of Microsatellite Polymorphisms for Genomewide Screening

All microsatellite markers and the methods for microsatellite analysis used in this study are described by Tamiya et al.[38] In brief, PCR primers were designed for amplifying fragments that include the microsatellite polymorphisms. All PCR primers were designed to have an annealing temperature of 57°C. Forward primers were labeled at the 5' end with fluorescent reagent (6-FAM or HEX [Applied Biosystems]). PCR on pooled DNAs was performed in 20-μl reactions containing 48 ng of pooled DNA, 0.5 units of DNA polymerase (AmpliTaq [Applied Biosystems]), 1 × reaction buffer with 1.5 mM MgCl$_2$ provided by the manufacturer (Applied Biosystems), 5 μM of each primer, and 0.25 mM of each deoxyribonucleotide triphosphate (dNTP) in 96- or 384-well plates. The amplification condition consisted of initial denaturation at 96°C for 5 min (hot start), annealing at 57°C for 1 min, and extension at 72°C for 1 min, followed by 40 cycles of denaturation at 96°C for 45 s, annealing at 57°C for 45 s, and extension at 72°C for 1 min, with use of a thermal cycler (GeneAmp PCR system 9700 [Applied Biosystems]).

For microsatellite typing of individual samples, PCR was performed in 12-μl reactions containing 2 ng of genomic DNA, 0.25 units of DNA polymerase (AmpliTaq Gold [Applied Biosystems]), 1 × reaction buffer with 1.5 mM MgCl$_2$ provided by the manufacturer, 5 μM of each primer, and 0.2 mM of each dNTP in 96- or 384-well plates. The amplification conditions were essentially the same as described above.

The PCR products were denatured in formamide (Hi-Di [Applied Biosystems]) at 95°C for 3 min and were separated by electrophoresis, with the use of an automated DNA sequencer with size standards (ABI Prism 3700 Genetic Analyzer, ROX size standard [Applied Biosystems]). The fragment size and the electrophoretograms were analyzed by GeneScan and Genotyper software (Applied Biosystems).

Additional Microsatellite Markers for High-Density Association Mapping

To obtain additional microsatellite markers in the narcolepsy candidate–region 1 (NLC1), the sequence of the candidate region was obtained from the University of California–Santa Cruz (UCSC) Genome Browser database (November 2002 version, based on NCBI Build 31). Then, the sequence was searched for repeated elements with the RepeatMasker program. Dinucleotide repeats with repeat number >12, trinucleotide repeats >8, and tetranucleotide to hexanucleotide repeats >5 were chosen. PCR primers were designed as described above, and we evaluated the polymorphism of each microsatellite with pooled DNA, searching for multiple peaks in the electrophoresis.

SNP Analyses

SNPs within the candidate region were selected from the Celera database at average intervals of ~5 kb, and specific PCR primers were designed. To confirm the polymorphisms of these SNP sites in the Japanese population, we examined 16 samples from patients with narcolepsy by direct sequencing, using a PCR cycle-sequencing kit and an automated DNA sequencer (BigDye Terminator v.3.1 Cycle Sequencing Kit and ABI PRISM 3730 DNA sequencer [Applied Biosystems]). The association analyses with these polymorphic sites were performed by direct sequencing of case and control samples.

The sequence of the entire region of *NLC1-A*, *NLC1-B*, and *NLC1-C* genes (based on NCBI Build 35 chromosome 21: 45234058–45250151) was also screened for polymorphisms with 16 samples, and polymorphic sites were subjected to association analyses by direct sequencing of case and control samples. Newly detected polymorphisms have been registered in the dbSNP database.

Expression Analysis by RT-PCR

The expression of the predicted genes in candidate region NLC1 was examined by RT-PCR, with the use of poly(A)⁺ RNA from the human brain, hypothalamus, peripheral blood, sperm, and several organs (i.e., heart, liver, spleen, pancreas, lung, kidney, and skeletal muscle [Bio Chain]). To discriminate PCR products derived from reverse-transcribed mRNA from those derived from genomic DNA, we designed specific forward and reverse primers in the predicted exon 1 and 2 regions, respectively. The primer sets for the predicted genes were as follows: 5'-CTAGGAGGGGAA-ACTGAGTCC-3' and 5'-CAGCACAGTTGGAGACATCACT-3' for *NLC1-A*, 5'-CCTCACAGCATCCCACATT-3' and 5'-TTTCTGGAAA-CAGCCAGGAG-3' for *NLC1-B*, and 5'-GCTGAACTGCCTGGACT-TTC-3' and 5'-ACATGTGCTCCCCACCTAAG-3' for *NLC1-C*. The thermal cycling profile consisted of initial denaturation at 96°C for 10 min, followed by 35 cycles of denaturation at 96°C for 45 s, annealing at 57°C for 45 s, extension at 72°C for 1 min, and a final extension at 72°C for 5 min, with the use of AmpliTaq Gold polymerase (Applied Biosystems). The PCR products were separated by electrophoresis on 2% agarose gels and were stained with ethidium bromide. The sequences of the amplified products were confirmed by direct sequencing.

Reporter-Gene Assay

Reporter-gene assays were performed using constructs containing microsatellite marker *D21S0012m* and SNP *rs13046884* alleles. For *D21S0012m*, genomic DNAs were obtained from four homozy-gotes for alleles with AC repeat numbers 8, 9, 10, and 12. A 908-bp fragment within the promoter region including *D21S0012m* was amplified by PCR, with use of the specific primers 5'-CAAAG-GTACCTCCAGTCCACACCCACC-3' and 5'-GTTTGAGCTCTTTG-GCCTGTCCATCAG-3'. Genomic DNA for SNP *rs13046884* alleles was obtained from one *rs13046884* heterozygote. A 297-bp fragment within *NLC1-A* intron 1, which includes *rs13046884*, was amplified using primers 5'-CAAAGGTACCAGGGTTGGACTCC-AAAGGGA-3' and 5'-GTTTGAGCTCGGGTGACTTCTTCACA-CCCA-3'. PCR was performed (TaKaRa LA *Taq* [TaKaRa]) with the following thermal cycling profile: denaturation at 96°C for 5 min, followed by 35 cycles at 96°C for 30 s, 60°C for 30 s, and 72°C for 1.5 min. PCR products were digested with *Sac*I and *Kpn*I restriction endonucleases and then were inserted upstream of a firefly luciferase gene in the pGL3-control vector (Promega), with the use of T4 DNA ligase (TaKaRa). Inserted sequences were confirmed by direct sequencing with primers specific to the pGL3-control vector (5'-CATACGCTCTCCATCAAAACAA-3' and 5'-AAGCCTCCTCACTACTTCTGGA-3'). The neuroblastoma cell line NB-1 and HeLa cells were maintained in accordance with published recommendations (Human Science Research Resources Bank). Then, 0.2 μg of each construct was introduced into the cells by a lipofection method (Effectene Transfection Reagent [Qiagen]), along with 0.02 μg of pRL-SV40 (Promega) as an internal control. Luciferase levels were determined using the DUAL-Luciferase Reporter Assay System (Promega), and firefly luciferase levels were normalized to the levels of renilla luciferase from pRL-SV40.

Statistical Analyses

Disease associations with polymorphisms were assessed by Fisher's exact test, with the use of 2×2 contingency tables for each allele. The smallest P value for each marker was selected. Allele frequencies in pooled-DNA typing were estimated from the height of peaks: each allele frequency was determined by dividing the height of each allele by the summed height of all alleles. In individual typing, the significance was evaluated by Fisher's exact test, with the use of $2 \times m$ (where m is the number of alleles) and 2×2 contingency tables. The significance level was set at .05 throughout this study, except for homogeneity among samples used in the first, second, and third set, which was tested by means of the Q statistic and was considered significant for $P < .10$.[39]

To assess the extent of pairwise linkage disequilibrium (LD) between polymorphisms, Lewontin's[40] D' and r^2 were calculated using a commercial software package (SNPAlyze-3.2 pro [Dyna-com]) based on the expectation-maximation algorithm. D' and r^2 were calculated only for polymorphisms with a minor-allele frequency (MAF) >6%. Pairwise D' and r^2 were plotted at the Cartesian coordinate corresponding to the polymorphism location on the physical map with the use of the GOLD program, as described by Abecasis and Cookson.[41]

Results

Genomewide Association Study

The 23,244 microsatellite markers used in the genome-wide association study are summarized in table 1. To reduce the cost and the technical burden of genomewide association analysis, the DNA-pooling method was applied in the first and second screenings (fig. 1A). Allele

frequencies were estimated from the height of individual peaks. To avoid false-negative associations, we performed no correction for multiple comparisons. Figure 1*B* shows the results of the association analyses in the first screening; the results for the 1,265 microsatellite markers on chromosome 6, which includes the *HLA* region, were described elsewhere.[36] A total of 2,686 markers (202 of which were on chromosome 6) showed significantly different frequencies between cases and controls. These 2,686 markers were further analyzed in the second screening with pooled DNA samples from different sets of cases and controls, and 96 markers (16 on chromosome 6) remained significantly different between cases and controls and had similar peak patterns between first and second case pools and between first and second control pools.

To confirm the associations observed, we subjected the 80 microsatellite markers located outside of chromosome 6 to individual typing with 95 case and 95 control samples, which were randomly chosen from the samples used in the first and second pools. Thirty markers still showed statistically significant differences by Fisher's exact test, with the use of 2 × 2 contingency tables (fig. 1*A* and 1*B* and table 2). In particular, 11 microsatellite markers also showed differences in allele frequencies with the use of 2 × *m* contingency tables. The remaining samples that were used in the first and second screenings (125 cases and 325 controls) were also genotyped for those 11 markers, and all the markers still reached a significant level. In addition, the smallest *P* values calculated by Fisher's exact test, with the use of 2 × 2 contingency tables in the pooled-DNA genotyping (first and second screenings), were reflected by the smallest *P* values in the individual genotyping with 220 cases and 420 controls.

One of the strong associations with narcolepsy was displayed by the microsatellite marker *D21S0241i*, located on 21q22.3 (based on NCBI Build 35 chromosome 21: 45169766–4516982S; [AAGG]$_{2-17}$). The frequency of the (AAGG)$_{10}$ allele was 8.6% among cases and 4.0% among controls (*P* = .0012; odds ratio [OR] 2.24; 95% CI 1.40–3.58). To further confirm the association, we tested *D21S0241i* for association in a third set of individuals not used in either of the pools (150 cases and 190 controls). Significant association was not observed in this set (*P* = .12; OR 2.11; 95% CI 0.88–5.06), but no heterogeneity was detected among the three sets of cases or controls by the Q statistic (*P* = .92), and the allele frequencies in the third set displayed the same general pattern among cases compared with controls as they did in the first and second sets. Moreover, the significant association was still observed when the association analysis was performed by

individual genotyping of the three sets of case and control samples (*P* = .00064; OR 2.08; 95% CI 1.38–3.13) (table 3). Taken together, these observations indicate that marker *D21S0241i* is associated with human narcolepsy.

High-Density Association Mapping with Additional Microsatellite Markers and SNPs

We analyzed the region surrounding the marker *D21S0241i* by high-density association mapping with additional microsatellite markers. To develop additional markers, we searched the surrounding genomic sequence for microsatellites. Polymorphisms of individual microsatellites were detected using pooled DNA samples, and 14 new microsatellite markers were established within 652 kb around marker *D21S0241i* (fig. 2*A*). These markers were analyzed in 220 case and 440 control samples (table 4). The new marker, *D21S0012m* (chromosome 21: 45238835–45238862), which is 70 kb from *D21S0241i*, showed a stronger association than *D21S0241i* (frequencies of the [AC]$_{in}$ allele: cases 0.9%, controls 4.6%; *P* = .00023; OR 0.19; 95% CI 0.074–0.48).

Next, to further define the candidate region, we performed high-density mapping with SNPs (listed in appendix A [online only]). To cover a 171-kb region around the markers *D21S0241i* and *D21S0012m*, we selected, from databases, SNPs at ~5-kb intervals. Direct sequencing on 16 cases (8 homozygotes and 8 heterozygotes of *D21S0012m* allele [AC]$_{10}$) was performed to screen for the SNPs. In total, 64 registered SNPs and 10 novel ones were identified and were subjected to association analyses with 190 cases and 190 controls (fig. 2*B*). Of the SNPs near *D21S0241i*, only one (*rs12483718*) showed a significant difference between cases and controls, whereas eight SNPs located close to *D21S0012m* showed significant differences. The strongest association with narcolepsy was exhibited by SNPs *rs13048981* and *rs13046884*, both located close to *D21S0012m* (for *rs13048981*, *P* = .0016, OR 0.17, and 95% CI 0.057–0.51; for *rs13046884*, *P* = .0010, OR 0.16, and 95% CI 0.055–0.48) (see fig. 3). The SNPs *rs13048981* and *rs13046884* were further typed for all the available samples (370 cases and 610 controls). The results for *rs13048981* were *P* = .00039, OR 0.31, and 95% CI 0.16–0.60; the results for *rs13046884* were *P* = .00036, OR 0.33, and 95% CI 0.18–0.62 (table 3). The two SNPs were further analyzed in 125 independently collected *HLA-DRB1*1501*–positive unaffected controls. Both SNPs again exhibited significant associations in the 370 cases compared with these controls (for *rs13048981*, *P* = .017, OR 0.33, and 95% CI 0.14–0.77; for *rs13046884*, *P* = .023, OR 0.36, and 95% CI 0.16–0.83) (table 3). Therefore, we considered this region to be a candidate region for susceptibility/resistance to human narcolepsy and tentatively named the region "narcolepsy candidate–region 1 (NLC1)."

The LD structure in this region was analyzed using the SNPs with MAFs >6%, and one large LD block was found (fig. 3*A* and 3*B*). SNPs *rs13048981* and *rs13046884* and

A

Association analysis using 23,244 MSs[a] with 1st set pooled DNAs
(cases: 110, controls: 210)

Assessment of reproducibility using 2,686 MSs with 2nd set pooled DNAs
(cases: 110, controls: 210)

Confirmation of association by individual genotyping for 80 MSs[b]
(cases: 95, controls: 95)[c]

Significant associations for 30 MSs

Association analyses for 11 MSs[d]
(cases: 220, controls: 420)[e]

D21S0241i was further examined with the 3rd set
(cases: 150, controls: 190)

High-density mapping around D21S0241i
using 14 additional MSs and 74 SNPs
(cases: 190, controls: 190)[e]

D21S0012m, rs13046884, and rs13048981 were examined in all samples
(cases: 370, controls: 610)

Association analyses for newly detected polymorphisms in NLC1 region
(cases: 190, controls: 190)[e]

Expression analyses of NLC1-A,-B, and -C by RT-PCR
and reporter-gene assay

B

$P = .05 \rightarrow$
$P = .001 \rightarrow$

chr.1 chr.2 chr.3 chr.4
chr.5 chr.6 chr.7 chr.8 chr.9
chr.10 chr.11 chr.12 chr.13 chr.14 chr.15 chr.16
chr.17 chr.18 chr.19 chr.20 chr.21 chr.22 chr.X chr.Y

Figure 1. Genomewide association analyses with 23,244 microsatellite markers. A, Flow chart of this study. a, MS = microsatellite marker. b, Sixteen MSs on chromosome 6 and 80 MSs on other chromosomes showing reproducible peak patterns and remaining significantly different between cases and controls. c, Selected randomly from the samples used in the first and second screenings. d, Eleven MSs reaching significance in both 2×2 and $2 \times m$ contingency tables. e, All samples used in first and second screenings. B, Results of genomewide screening. The figure shows P values by Fisher's exact test based on 2×2 contingency tables (green line) or on $2 \times m$ contingency tables (red line) in the first screening. Yellow circles indicate 30 MSs that showed significant associations in both first and second screenings and in individual typing.

Table 2. Thirty Microsatellite Markers Showing Significant Association in the First and Second Screenings and in the Subsequent Individual Genotyping

				P			
		Pooled DNA[a]		95 Cases and 95 Controls		220 Cases and 420 Controls	
Marker	Chromosome	First	Second	2×2[b]	$2 \times m$[c]	2×2[b]	$2 \times m$[c]
D1S0500i	1q23.1	.046	.00024	.017	.28	...	...
D1S0583i	1q32.2	.038	.049	.018	.11	...	...
D1S1208i	1q32.2	.045	.045	.029	.034	.0010	.0027
D1S1148i	1q31.2	.025	.047	.018	.073	...	...
D2S303	2p14	.045	.017	.021	.19	...	...
D2S0878i	2p16.2	.0011	.025	.0023	.0020	.0010	.00073
D3S0502i	3p22.2	.019	.036	.037	.15	...	...
D3S0971i	3q22.2	.037	.016	.031	.23	...	...
D3S0978i	3q24	.0031	.0047	.0044	.041	.0081	.13
D3S1174i	3p14.1	.044	.027	.022	.0084	.0021	.0013
G08391	4p15.1	.041	.047	.044	.16	...	...
D4S0140i	4p15.1	.0027	.037	.0023	.0067	.0020	.0070
D4S0424i	4p16.3	.038	.036	.049	.63	...	...
D5S0022i	5q32	.012	.0084	.0040	.016	.011	.0017
D5S0565i	5p13.3	.0051	.013	.0031	.052	...	...
D7S0486i	7p15.2	.036	.0020	.049	.68	...	...
D7S0760i	7p11.2	.0044	.0040	.016	.086	...	...
D7S1066i	7q11.22	.0089	.028	.011	.095	...	...
D8S0068i	8	.018	.034	.011	.30	...	...
D8S0584i	8q24.21	.012	.012	.018	.11	...	...
D14S0284i	14q31.3	.0030	.049	.0058	.018	.027	.38
D15S150	15q21.3	.020	.049	.024	.21	...	...
D15S0157i	15q21.3	.019	.0088	.010	.16	...	...
D17S1300	17q24.3	.022	.0071	.036	.13	...	...
D17S0179i	17	.0044	.050	.018	.0090	.0016	.0060
D17S0306i	17p11.2	.0060	.021	.011	.014	.0069	.076
D20S0027i	20p11.21	.0055	.014	.024	.18	...	...
D21S0098i	21q21.1	.023	.0044	.00029	.0051	.00031	.011
D21S0241i	21q22.3	.018	.00043	.0098	.018	.0012	.048
DXS0660i	Xp22.13	.00061	.0080	.0025	.065	...	...

[a] P values calculated by Fisher's exact test, based on 2×2 contingency tables with estimated allele frequencies. The smallest P value was selected. The alleles that showed the smallest P values in the pooled DNA genotypings were reflected in the individual genotyping.

[b] P values calculated by Fisher's exact test, based on 2×2 contingency tables. The smallest P value was selected.

[c] P values calculated by Fisher's exact test, based on $2 \times m$ contingency tables.

microsatellite marker D21S0012m were in the same LD block, whereas D21S0241i was not. In addition, the rs13046884 g allele, the rs13048981 t allele, and the D21S0012m (AC)$_{10}$ allele were found to be in strong LD ($r^2 > 0.94$), and the estimated haplotype frequency was 4.5% in the controls.

The region around the three polymorphisms contains three predicted genes registered in the UCSC Genome Browser, each of which is supported by between two and five mRNAs or ESTs (fig. 2C). These predicted genes are on the reverse strand on chromosome 21q22.3, with positions as follows: NLC1-A 45234209–4523842, NLC1-B 45238709–45239923, and NLC1-C 45243550–45249070 (Genome Browser accession numbers BC036902, BC009635, and BC027456, respectively). According to the UCSC Genome Browser, NLC1-A produces two alternatively spliced transcripts encoding different protein isoforms; the position of the short isoform is 45235619–45238383. The functions of these predicted genes are currently unknown.

We performed further variation screening on the three genes by direct sequencing with 16 samples, and 26 polymorphisms were observed. Fourteen of the polymorphisms were new: eight SNPs in NLC1-A, two in NLC1-B, and four in NLC1-C. Next, these new polymorphisms were subjected to association analysis with 190 cases and 190 controls (fig. 2C). Four SNPs reached significance in the analysis, but none was stronger than rs13048981 or rs13046884, indicating that these two SNPs, as well as D21S0012m, are associated primarily in this region.

Table 3. Association Analyses of *D21S0241i, D21S0012m, rs13048981,* and *rs13046884* with 370 Patients with Narcolepsy and 610 Unaffected Controls

	No. (%) of Individuals		
Marker or SNP and Allele	Patients with Narcolepsy (n = 370)	Control Individuals (n = 610)	DRB1*1501-Positive Control Individuals (n = 125)
D21S0241i:			
$(AAGG)_7$	0 (.0)	1 (.1)	...
$(AAGG)_8$	0 (.0)	1 (.1)	...
$(AAGG)_9$	1 (.1)	0 (.0)	...
$(AAGG)_{10}$ *	51 (6.9)	42 (3.4)	...
$(AAGG)_{11}$	65 (8.8)	90 (7.4)	...
$(AAGG)_{12}$	155 (20.9)	258 (21.1)	...
$(AAGG)_{13}$	154 (20.8)	249 (20.4)	...
$(AAGG)_{14}$	195 (26.4)	359 (29.4)	...
$(AAGG)_{15}$	94 (12.7)	180 (14.8)	...
$(AAGG)_{16}$	24 (3.2)	35 (2.9)	...
$(AAGG)_{17}$	1 (.1)	5 (.4)	...
D21S0012m:			
$(AC)_8$	127 (17.2)	168 (13.8)	...
$(AC)_9$	447 (60.4)	762 (62.5)	...
$(AC)_{10}$ *	12 (1.6)	54 (4.4)	...
$(AC)_{11}$	36 (4.9)	48 (3.9)	...
$(AC)_{12}$	117 (15.8)	188 (15.4)	...
$(AC)_{13}$	1 (.1)	0 (.0)	...
rs13048981:			
Genotype[c,d]:			
CC	360 (97.3)	561 (92.0)	115 (92.0)
CT	10 (2.7)	47 (7.7)	10 (8.0)
TT	0 (.0)	2 (.3)	0 (.0)
Allele[e,f]:			
C	730 (98.6)	1,169 (95.8)	240 (96.0)
T	10 (1.4)	51 (4.2)	10 (4.0)
rs13046884:			
Genotype[g,h]:			
AA	359 (97.0)	559 (91.6)	115 (92.0)
AG	11 (3.0)	49 (8.0)	10 (8.0)
GG	0 (.0)	2 (.3)	0 (.0)
Allele[i,j]:			
A	729 (98.5)	1,167 (95.7)	240 (96.0)
G	11 (1.5)	53 (4.3)	10 (4.0)

[a] OR 2.08; 95% CI 1.4–3.1; $P = .00064$.

[b] OR 0.36; 95% CI 0.2–0.7; $P = .00068$.

[c] $P = .00095$ (patients with narcolepsy compared with controls, by Fisher's exact test based on a 2 × 3 contingency table).

[d] $P = .016$ (patients with narcolepsy compared with DRB1*1501-positive controls, by Fisher's exact test based on a 2 × 3 contingency table).

[e] OR 0.31; 95% CI 0.16–0.60; $P = .00039$ (patients with narcolepsy compared with controls, by Fisher's exact test based on a 2 × 2 contingency table).

[f] OR 0.33; 95% CI 0.14–0.77; $P = .017$ (patients with narcolepsy compared with DRB1*1501-positive controls, by Fisher's exact test based on a 2 × 2 contingency table).

[g] $P = .0011$ (patients with narcolepsy compared with controls, by Fisher's exact test based on a 2 × 3 contingency table).

[h] $P = .022$ (patients with narcolepsy compared with DRB1*1501-positive controls, by Fisher's exact test based on a 2 × 3 contingency table).

[i] OR 0.33; 95% CI 0.18–0.62; $P = .00036$ (patients with narcolepsy compared with controls, by Fisher's exact test based on a 2 × 2 contingency table).

[j] OR 0.36; 95% CI 0.16–0.83; $P = .023$ (patients with narcolepsy compared with DRB1*1501-positive controls, by Fisher's exact test based on a 2 × 2 contingency table).

Expression Analyses

We assessed the expression of these three predicted genes in the human brain, hypothalamus, and other organs by RT-PCR, using specific primers (fig. 4A). Products with the expected size were amplified for *NLC1-A* and *NLC1-C* in whole brain and hypothalamus (fig. 4B and 4C). Moreover, direct sequencing of the products confirmed that the correct sequence was amplified. However, for *NLC1-B*, the amplified band was from genomic DNA, not from cDNA. These observations indicate that *NLC1-A* and *NLC1-C* were expressed in human whole brain and hypothalamus, whereas *NLC1-B* was not. Notably, *NLC1-A* was also expressed in human spleen, lung, kidney, and skeletal muscle, and *NLC1-C* was also expressed in human spleen, pancreas, lung, and sperm (fig. 4C), but neither was expressed in peripheral blood (data not shown). SNP *rs13046884* is

Table 4. Association Analyses with High-Density Microsatellite Markers around Marker *D21S0241i*

The table is available in its entirety in the online edition of *The American Journal of Human Genetics*.

in *NLC1-A* intron 1, and *D21S0012m* is 424 bp upstream of the transcriptional start site of *NLC1-A*, which suggests that *NLC1-A* may be a susceptibility/resistance gene for human narcolepsy. SNP *rs13048981* is located 2,602 bp upstream of *NLC1-B*, which was not expressed in human brain, and its position, 4,164 bp upstream of *NLC1-A*, suggests that its association with narcolepsy resulted merely from the LD with *rs13046884* and *D21S0012m*. Thus, it is unlikely that *NLC1-B* is a susceptibility/resistance gene for human narcolepsy.
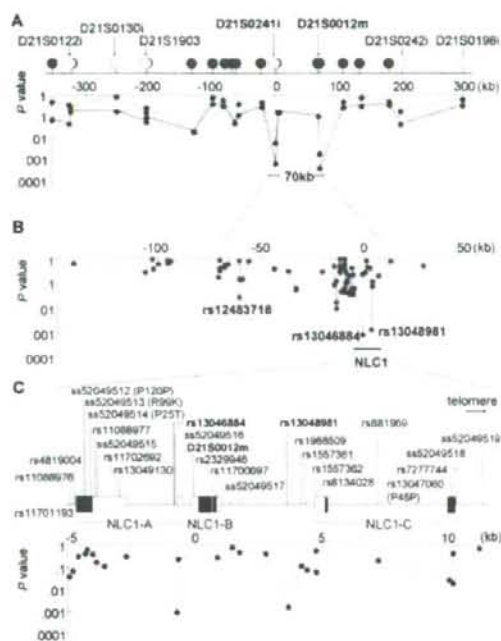

Figure 2. High-density mapping with additional microsatellite markers and SNPs. *A*, Association analyses using high-density microsatellite markers with 220 cases and 420 controls. Unblackened circles indicate microsatellite markers used in the first and second screenings. Blackened circles indicate microsatellite markers newly developed for the high-density mapping. The dark line shows the *P* values calculated by Fisher's exact test based on 2 × 2 contingency tables, whereas the lighter line shows those from 2 × *m* contingency tables. *B*, Association analyses using SNPs with 190 cases and 190 controls. The *X*-axis indicates the distance from *D21S0012m*. SNP *rs12483718* is located near *D21S0241i*. The *Y*-axis shows the *P* values calculated by Fisher's exact test based on 2 × 2 contingency tables. Two SNPs, *rs13048981* and *rs13046884*, showed the strongest associations in the NLC1 region. *C*, Variation screening and high-density association analyses in the NLC1 region. *Top*, Exon-intron structures of *NLC1-A*, *NLC1-B*, and *NLC1-C*. Boxes indicate exons, with unblackened boxes indicating untranslated regions and blackened boxes indicating coding regions. Predicted gene regions and 1 kb of upstream region were screened for sequence variations. Fourteen additional polymorphisms, including two nonsynonymous substitutions, were detected and were examined for possible associations, but no polymorphisms showed stronger association than *D21S0012m*, *rs13048981*, and *rs13046884*. *Bottom*, *P* values for individual SNPs.

– 124 –